PCCP

PAPER

View Article Online
View Journal | View Issue

Cite this: *Phys. Chem. Chem. Phys.*, 2025, **27**, 9864

Indications for a universal hydrogen catalysis mechanism in [FeFe]-hydrogenases of different phylogenetic groups†

Moritz Senger, *[ab] Conrad Schumann, [a] Princess R. Cabotaje, [a] Afridi Zamader, ‡[a] Ping Huang, [a] Henrik Land [a] and Gustav Berggren *[a]

[FeFe]-hydrogenases are metalloenzymes catalysing bidirectional hydrogen (H_2) turnover. These enzymes are generally considered to be extremely efficient and fast catalysts. However, [FeFe]-hydrogenases constitute a very diverse enzyme family that can be divided into several distinct phylogenetic groups, denoted as groups A–G. Very little is known about the properties of [FeFe]-hydrogenases outside of the intensively studied group A, but recent studies on putatively sensory group C and D enzymes have revealed distinct differences in reactivity. The variation in structure, reactivity and physiological function observed between phylogenetic groups raises the question if all [FeFe]-hydrogenases follow the same mechanism for H_2 turnover. Here, we provide the first detailed spectroscopic investigation of a slow-acting putatively sensory group D [FeFe]-hydrogenase from *Thermoanaerobacter mathranii* (*Tam*HydS). Photo-reduction enabled us to characterize redox states in group D [FeFe]-hydrogenase *via* infrared spectroscopy under catalytic conditions. The sequential population of redox states similar to group A [FeFe]-hydrogenases supports the notion that group A and D [FeFe]-hydrogenases follow a universal catalytic mechanism. However, clear differences between enzymes from different phylogenetic groups become evident when comparing the relative stability and protonation state of suggested key catalytic intermediates. Moreover, the spectroscopic data collected on *Tam*HydS provides new insight into the structure of the reduced active site, lending further support for the notion of a retained bridging CO ligand throughout the entire catalytic cycle.

Received 31st January 2025,
Accepted 16th April 2025

DOI: 10.1039/d5cp00412h

rsc.li/pccp

Introduction

[FeFe]-hydrogenases are metalloenzymes involved in hydrogen metabolism. They are a structurally and functionally highly diverse enzyme family and can be classified into phylogenetic groups (denoted group A–G).[1] Outside of group A, there is limited data available on [FeFe]-hydrogenases. Still, group C and D [FeFe]-hydrogenases stand out as they are proposed to serve a H_2 sensory function rather than a catalytic one.[2,3] The different phylogenetic groups likely share the same organometallic catalytic cofactor but differ in the active-site pocket and substrate transport pathways.[2,4] The active site consists of a unique diiron site with a terminal CO and CN^- ligand at each iron ion. The iron ions are further coordinated by two bridging ligands, a bidentate azadithiolate (–SCH_2NCH_2S–, ADT) and an additional CO molecule (μCO). The diiron site is linked *via* a cysteine residue to a [4Fe–4S] cluster ($[4Fe–4S]_H$) to form the so-called H-cluster (Fig. 1A). Many [FeFe]-hydrogenases harbour additional [4Fe–4S] clusters in the N terminal domain involved in electron transfer, commonly denoted as F-clusters. In addition, group C and D enzymes often harbour an additional FeS cluster in the C-terminal domain called C-clusters. Due to their outstanding catalytic properties, [FeFe]-hydrogenases and the H-cluster have received significant attention from the bioinorganic chemistry and solar fuel research communities.[5–8]

To-date, mechanistic investigations have focused almost exclusively on group A [FeFe]-hydrogenases, for which several protonation and oxidation states of the H-cluster have been characterized. Albeit the mechanism remains debated, all currently proposed catalytic cycles include oxidized, single and double reduced H-cluster states.[15–17] Multiple spectroscopic signals associated with such states have been identified by Fourier-transform infrared (FTIR) and electron paramagnetic

[a] *Department of Chemistry – Ångström Laboratory, Molecular Biomimetics, Uppsala University, 75120 Uppsala, Sweden. E-mail: moritz.senger@kemi.uu.se, gustav.berggren@kemi.uu.se*
[b] *Department of Chemistry – BMC, Biochemistry, Uppsala University, 75120 Uppsala, Sweden*

† Electronic supplementary information (ESI) available. See DOI: https://doi.org/10.1039/d5cp00412h

‡ Current address: Laboratoire d'Electrochimie Moléculaire (LEM), Université Paris Cité, CNRS, F-75006, Paris, France.

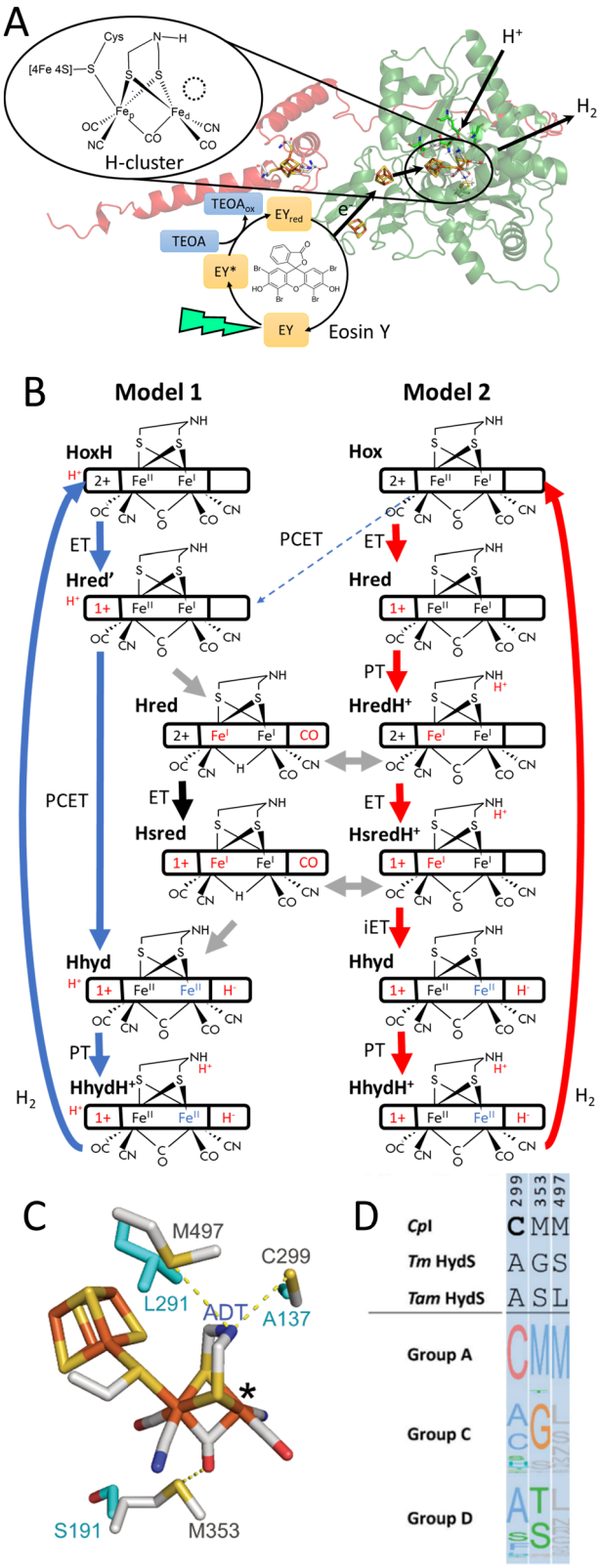

Fig. 1 (A) *Tam*HydS protein structure, H-cluster and photo-reduction scheme. YASARA-generated homology model (green cartoon) of *Tam*-HydS[9,10] based on the crystal structure of CpI (PDB ID 4XDC[11]). The [4Fe–4S] clusters and the H-cluster are shown as sticks (C: gray, Fe: orange, S: yellow, N: blue, O: red) The additional C-terminal domain was predicted with Alphafold (red cartoon) and the associated [4Fe–4S] cluster inserted manually. Details are described in the *Tam*HydS structure section in the ESI.† Eosin Y (EY) is excited by visible light (EY*) and reductively quenched by triethanolamine (TEOA). The reduced Eosin Y (EY_{red}) can donate electrons to *Tam*HydS resulting in population of reduced states and eventually H_2 production. (B) Two main catalytic cycle models. Model 1 blue arrows, model 2 red arrows, grey arrows indicate ligand rotation. The CO ligand occupying the apical vacancy and bound protons are indicated in red. Electron transfer (ET), internal electron transfer (iET), proton transfer (PT) and proton coupled electron transfer (PCET) steps are indicated at the arrows. Red letters indicate the site of reduction, blue letters the site of oxidation relative to the oxidized state (H_{ox}). Note that for model 2 the nomenclature introduced by Sommer *et al.*[12] is used which leads to different redox states having the same abbreviation. (C) Group A and D cofactor second coordination sphere differences. Amino acids of *Cp*I interacting with the H-cluster (C299, M353, and M497) are shown in sticks (grey: C, yellow: S). The azadithiolate (ADT) bridgehead is labelled as blue text. Hydrogen turnover is catalysed at the distal iron denoted as Fe_d (*). The corresponding residues from the homology model of *Tam*HydS are overlaid (cyan: C, red: O). (D) Normalized consensus logos of groups A, C, and D [FeFe]-hydrogenase generated in Jalview using ClustalΩ[13] sequence alignment of sequences retrieved from Greening *et al.*[14] The numbering is based on the sequence of *Cp*I. The conservation of the amino acid in a position is proportional to its font size.

resonance (EPR) spectroscopy. The oxidized state (H_{ox}) features a $[4Fe–4S]_H^{2+}$ cluster and a Fe(II)Fe(I) diiron site. The H_{ox} state and its potentially protonated equivalent $H_{ox}H$, feature the aforementioned bridging CO ligand.[18] This ligation results in an open coordination site in an apical position at the distal iron atom (Fe_d), a structure defining the "rotated" diiron site geometry.[19–22] The first reduction occurs at the $[4Fe–4S]_H$ cluster forming the H_{red}' state.[12,18,23] Protonation coupled to intramolecular electron transfer from the $[4Fe–4S]_H$ cluster to the diiron site has been proposed to give rise to a diiron site reduced state denoted H_{red} (sometimes $H_{red}H^+$). Addition of a second electron to the H-cluster gives rise to the "super-reduced" state H_{sred} (or $H_{sred}H^+$), with a reduced $[4Fe–4S]_H^+$ cluster. The hydride state, H_{hyd}, is a tautomer of H_{sred} featuring a terminal hydride at the former apical vacancy giving a formally di-ferrous diiron site.[24–26] Protonation of H_{hyd} at the amine of the ADT ligand is proposed to yield the still only partially characterized state, $H_{hyd}H^+$.[27,28] The hydride and the proton may form H_2, returning the H-cluster to the oxidized state, H_{ox}. The exact structure and catalytic relevance of these states are subject to ongoing discussion, which has resulted in competing mechanistic models, at least two of which are extensively reviewed in recent literature.[2,5,16,29–31]

In short, the two mechanistic models diverge in the interpretation of the spectroscopic data, both with regards to ligand geometry of the diiron subsite as well as protonation status of the H-cluster (Fig. 1B). In model 1, two of the aforementioned reduced states, H_{red} and H_{sred}, are interpreted as inhibited states adopting an "inverted" diiron site geometry. Critically, here protonation of the diiron subsite is proposed to occur at the Fe ions yielding a bridging hydride (μH), while the former μCO ligand shifts to a terminal position that otherwise provides the apical vacancy. The expected thermodynamic stability of the μH geometry,[32,33] and the additional ligand rotation necessary to form a terminal hydride disfavour their involvement in fast H_2 catalysis.[30,34–36] Conversely, in model 2, the same

spectroscopic signals are attributed to species protonated at the ADT-amine instead of the iron ions, and commonly denoted $H_{red}H^+$ and $H_{sred}H^+$. As a consequence, $H_{red}H^+$ and $H_{sred}H^+$ are proposed to retain the rotated geometry of the H_{ox} state and to be catalytically relevant.[12,16] In favour of model 1, the absence of a μCO band for H_{red} has been noted in numerous independent studies. An observation which, coupled with comprehensive DFT calculations and isotope editing, supports the notion of an inverted geometry in H_{red}.[34,35] However, low temperature experiments provide support for model 2. Albeit the μCO ligand band expected for the $H_{red}H^+$ state has proven challenging to observe at room temperature it has been detected *via* FTIR spectroscopy at cryogenic temperatures.[37–39]

In the following, we will use the $H_{red}'/H_{red}/H_{sred}$ nomenclature to define specific spectroscopic fingerprint signals, without implying a specific ligand geometry and/or protonation status.

It is well-established that the protein environment has a large effect on the H-cluster.[17,40–42] In group A [FeFe]-hydrogenases both the active-site pocket and a proton transfer pathway (PTP), composed of conserved amino acids and water molecules, are supposed to play a key role in fast catalysis.[43–45] The H-bonding partners of the CN^- ligands of the H-cluster are conserved in the vast majority of groups of [FeFe]-hydrogenases.[1,46] Beyond these immediate interactions, several outer-coordination sphere amino acid residues are strictly conserved in the active-site pocket of group A [FeFe]-hydrogenases. Variation of these conserved residues through site directed mutagenesis has been shown to significantly impair turnover rates and in some cases even prevent H-cluster assembly.[40] However, the putatively sensory enzymes in groups C and D display variations of several conserved amino acids constituting the outer-coordination sphere in group A [FeFe]-hydrogenases (Fig. 1C and D).[3,9] Moreover, the PTP of group A is not conserved in either group C or group D [FeFe]-hydrogenases, and a distinct alternative PTP has been proposed for group D.[47]

As expected from these structural differences, the reactivity of group C and D enzymes is clearly different from the well-known group A [FeFe]-hydrogenases. Activity assays have shown that group C and group D enzymes are significantly slower than any reported group A enzyme.[3,9] Introducing the PTP and active-site of group A [FeFe]-hydrogenase into a group D enzyme has been shown to increase the catalytic rate more than 100-fold, underscoring the impact of the protein scaffold on H-cluster reactivity.[42] Moreover, an alternative diiron site reduced state Fe(I)Fe(I), denoted H^*_{red}, has so far been detected exclusively in spectro-electrochemistry studies of the group C [FeFe]-hydrogenase from *Thermotoga maritima* (*Tm*HydS).[3,48] Compared to $H_{red}H^+$, H^*_{red} is proposed to lack the additional protonation at the ADT while featuring the rotated, μCO, geometry (compare Fig. S1, ESI†). In the only characterized group D [FeFe]-hydrogenase, from *Thermoanaerobacter mathranii* (*Tam*HydS), catalysis is bidirectional but thermodynamically irreversible.[9] Kinetic modelling of cyclic voltammetry traces recorded under varied pH and H_2 pressure supports the notion that *Tam*HydS nevertheless follows the same mechanism as group A hydrogenases.[49,50] However, there is currently very limited spectroscopic data available for *Tam*HydS under turnover conditions to support this hypothesis. With regards to possibly catalytically active states, previously observed in group A enzymes, only oxidized ($H_{ox}/H_{ox}H$) and a one-electron reduced redox state (H_{red}) of the diiron site have been reported to-date.[9,10]

[FeFe]-hydrogenases serve as model systems for probing general concepts such as thermodynamically reversible *vs.* irreversible catalysis.[51] Thus, spectroscopic insight into the mechanism of these ''non-prototypical'' [FeFe]-hydrogenases is required to support or refute the suggestion arising from kinetic modelling work that the irreversible group D enzyme *Tam*HydS still follows the same mechanism as the reversible group A enzymes.[50] Furthermore, considering how the active site of [FeFe]-hydrogenases inspire the design of synthetic catalysts for sustainable H_2 catalysis,[5,6] a more detailed characterization of the group C and D enzymes is arguably critical to improve our understanding of how the outer-coordination sphere modulates the reactivity of the H-cluster.

Our initial efforts using spectro-electrochemistry and chemical reductants to probe the H-cluster of *Tam*HydS have only revealed interconversion between the H_{red} and H_{ox} states.[9] To gain further insight into the H-cluster chemistry under turnover conditions we instead applied photo-reduction. [FeFe]-hydrogenases are not intrinsically photoactive, but catalysis can be photo-triggered *via* a suitable photosensitizer (Fig. 1A). Such photo-reduction has been shown to induce H_2 catalysis *in vitro*[52–55] and in living cells.[56,57] Moreover, this technique has facilitated investigations into the population of the reduced state (H_{red}) of the H-cluster as well as associated changes in the proton transfer pathway (PTP) of group A [FeFe]-hydrogenases under both steady-state and time-resolved conditions.[45,57,58]

Here, we investigate the group D [FeFe]-hydrogenase *Tam*HydS *via* attenuated total reflection Fourier-transform infrared (ATR-FTIR) spectroscopy, complemented by electron paramagnetic resonance (EPR) spectroscopy. Through photo-reduction, we now have detected a variety of additional states that feature similar redox levels as in group A [FeFe]-hydrogenases. We observe the accumulation of four distinct diiron site reduced states that most likely differ in protonation chemistry, of which two were exclusively observed in the group C [FeFe]-hydrogenase *Tm*HydS before.[3] In turnover experiments, we can confirm a sequential population of redox states, namely from the oxidized state to one-electron reduced to two-electron reduced and putatively terminal hydride bound intermediates. Despite notable differences in active site cofactor environment, PTP, as well as catalytic activity rates, our findings provide support for a conserved catalytic mechanism in group A and D [FeFe]-hydrogenases. Additionally, the study sheds new light on the contested H_{red} intermediate.[16,29] The detection of a potential bridging CO ligand in the spectroscopic signature of the H_{red} state indicates that the catalytically important rotated cofactor geometry can be conserved for the reduced diiron site intermediate at ambient conditions.

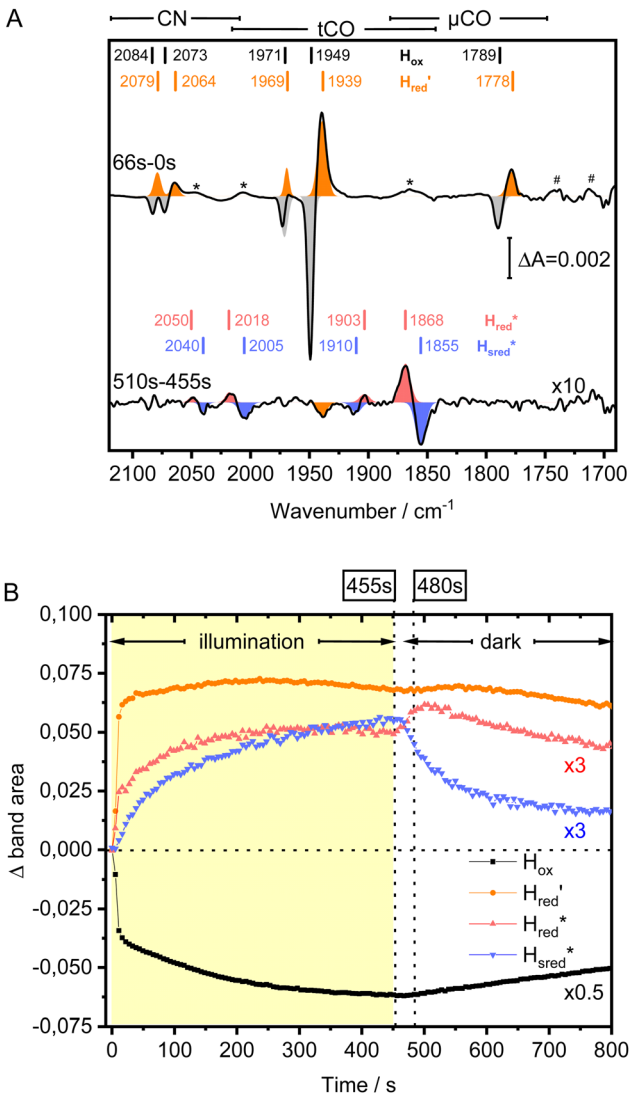

Fig. 2 (A) ATR-FTIR difference spectra of the *Tam*HydS^{PDT}/Eosin Y/TEOA mixture. Reduction upon illumination (66 s of illumination minus the initial pre-illumination "0 s" spectrum, top spectrum) and auto-oxidation after illumination was stopped (480 seconds minus the last illuminated spectrum at 455 seconds, bottom spectrum). The peaks of terminal cyanide (CN^-), terminal (tCO) and bridging carbon monoxide (μCO) ligands for different redox states are colour coded and the band patterns indicated by coloured bars. (Top spectrum) Upon photo-reduction the oxidized state (H_{ox}, 2084, 2073, 1971, 1949 and 1789 cm^{-1}) depopulates, predominantly in favour of the one-electron reduced state (H_{red}', 2079, 2064, 1969, 1939 and 1778 cm^{-1}). Potential bands indicated by # do not correlate with any of the band patterns observed here. (Bottom spectrum) The 10-fold magnified difference spectrum displays the changes during re-oxidation after illumination. The minor redox species indicated by an * in the top spectrum can be assigned to H_{red}^* (2050, 2018, 1903 and 1868 cm^{-1}) and H_{sred}^* (2040, 2005, 1910 and 1855 cm^{-1}). Compare with (B) for the kinetics of (de)-population during and after photo-reduction. (B) Redox state populations over time during and after photo-reduction. The time traces represent the sum of the difference peak area associated with a given redox state. To facilitate comparison the population of H_{red}^* and H_{sred}^* are multiplied by a factor of 3. The yellow box indicates the illumination period. Within 22 seconds most of the H_{ox} population (black) is converted into H_{red}' (orange). Half the H_{red}^* population (red) is formed on the same timescale. Subsequently, H_{sred}^* (blue) starts to accumulate. Directly after illumination H_{ox} and H_{red}' appear to remain constant while H_{sred}^* decays and H_{red}^* gets transiently populated. On a longer timescale > 150 seconds after illumination, all reduced species convert into H_{ox}. Compare Fig. S4 (ESI†) for zoom-ins on the direct changes upon illumination and after illumination.

Results and discussion

Spectroscopic investigation of group D [FeFe]-hydrogenase *Tam*HydS^{PDT}

We initially studied an artificially matured variant of *Tam*HydS where the secondary amine of the ADT bridgehead is replaced by a methylene group (PDT) denoted *Tam*HydS^{PDT} to avoid the complexity arising from protonation of the diiron subsite. For PDT cofactor variants of group A [FeFe]-hydrogenases, H_{ox} and H_{red}' are the main redox states reported.[59,60] A mixture of *Tam*HydS^{PDT} [FeFe]-hydrogenase, photosensitizer (Eosin Y), and sacrificial electron donor (triethanolamine (TEOA)) was applied to the surface of the ATR crystal, dried, and subsequently rehydrated with pH 8 Tris buffer. During continuous white light illumination, the photo-reduction of *Tam*HydS^{PDT} was followed in real time by ATR-FTIR difference spectroscopy. Fig. 2A (top spectrum) displays the "light minus dark" difference spectrum in the region of the CO and CN^- ligands of the diiron site. Before illumination, the sample adopted the oxidized resting state, H_{ox}, with its characteristic bands at 2084, 2073, 1971, 1949 and 1789 cm^{-1} (negative grey bands Fig. 2A). Upon photo-reduction, H_{ox} depopulates, converting into the commonly observed $[4Fe–4S]_H$ cluster reduced state, H_{red}', with bands at 2079, 2064, 1969, 1939 and 1778 cm^{-1} (positive orange bands Fig. 2A). The absolute spectra indicate that the transition is nearly quantitative (Fig. S2, ESI†). However, minor unassigned peaks in the difference spectrum indicate the formation of additional reduced species (marked by an * in Fig. 2A, top).

The origin of these minor contributions becomes clearer when studying the auto-oxidation of the enzyme, spontaneously occurring once illumination was stopped. The difference spectrum computed from a dark spectrum collected 55 s after stopping illumination and the last illuminated spectrum (time-points indicated by dashed lines in Fig. 2B) clearly shows that the unassigned features can be attributed to two additional interconverting states (Fig. 2A bottom spectrum). We observe positive bands at 2050, 2018, 1903 and 1868 cm^{-1} and negative bands at 2040, 2005, 1910 and 1855 cm^{-1}. In both band patterns, the lowest wavenumber band is the most intense, which is a characteristic of diiron site reduced states.[12,18,19] Since the PDT ligand cannot be protonated and the cofactor cannot yield H_{red} and H_{sred}, we assign the minor species with a pronounced absorbance feature at 1868 cm^{-1} to H_{red}^* (Fig. 2A, bottom spectrum, positive bands), in agreement with data reported for the group C [FeFe] hydrogenase *Tm*HydS^{PDT}.[3] It follows that the second minor component, which is lost upon incubation in darkness, is attributable to H_{sred}^* (compare Fig. S1, ESI†) additionally reduced at the $[4Fe–4S]_H$ cluster (Fig. 2A, bottom spectrum, negative bands). We do not observe the photolysis of CO ligands during photo-reduction.[61,62] Repeating the experiment with *Tam*HydS^{PDT} samples including sodium dithionite led to practically indistinguishable results (Fig. S3, ESI†). An overview of all *Tam*HydS infrared signatures is given in Table 1 and Fig. S9 (ESI†). The detailed fit parameters for all infrared signatures can be found in the ESI.†

Table 1 Infrared band patterns of different redox states in *Tam*HydS (group D) and *Cr*HydA1 (group A) or *Tm*HydS (group C) [FeFe]-hydrogenase

	*Tam*HydS (group D) bands in cm^{-1}	*Cr*HydA1 (group A) bands in cm^{-1}
H_{ox}	2082, 2074, 1970, 1948, 1787[9]	2088, 2072, 1964, 1940, 1800[25]
$H_{ox}H$	n.d., n.d., 1978, 1954, 1795[9]	2092, 2072, 1970, 1946, 1812[18]
H_{red}	2062, 2030, 1961, 1922, 1895[9]	2072, 2033, 1961, 1915, 1891[35]
	2062, 2032, 1922, 1896, 1803 (this study)	At 90 K, n.d, n.d., 1919, 1891, 1817[39]
H^*_{red}	2052, 2012, 1903, 1875, n.d. (this study)	#*Tm*HydS^{ADT} (group C) 2055, 2022, 1894, 1871, 1763[3]
H^{*PDT}_{red}	2050, 2018, 1903, 1868, n.d. (this study)	#*Tm*HydS^{PDT} (group C) 2048, 2012, 1883, 1862, n.d.[3]
$H_{red}{}'$	n.d, n.d., 1960, 1939, 1782 (this study)	2084, 2066, 1962, 1933, 1792[15]
H'^{PDT}_{red}	2079, 2064, 1969, 1939, 1778 (this study)	2090, 2072, 1966, 1941, 1810[59]
H_{sred}	n.d., n.d., 1912, 1887, n.d. (this study)	2068, 2026, 1953, 1918, 1882[35]
H^*_{sred}	n.d., n.d., n.d.,1865, n.d. (this study)	#*Tm*HydS^{ADT} (group C) 2047, 2013, 1900, 1861, 1751[3]
H^{*PDT}_{sred}	2040, 2005, 1910, 1855, n.d. (this study)	#*Tm*HydS^{PDT} (group C) 2042, 2007, 1894, 1853, n.d.[3]
H_{hyd}	2082, 2075, 1981, 1970, 1848 (this study)	2082, 2068, 1978, 1960, 1860[24]

Bands are indicated in the order CN, CN, tCO, tCO, μ/tCO. #Data reported for the group C enzyme *Tm*HydS is listed for H^*_{red} and H^*_{sred} to compare the observed band positions since this is the only [FeFe]-hydrogenases previously reported to adopt these states.

Using the aforementioned redox state assignment, we can monitor the redox state population over time during and after photo-reduction (Fig. 2B). A rapid conversion of H_{ox} primarily into $H_{red}{}'$ is evident during the first 22 seconds of illumination. H^*_{red} also starts to accumulate rapidly, reaching approximately half of the final H^*_{red} population on the same timescale (Fig. S4 for zoom in, ESI†). However, while the $H_{red}{}'$ population appears to plateau, we observe further population of H^*_{red} on a longer timescale. A lag-phase of about 20 seconds is observed for the population of H^*_{sred}. The fact that H^*_{sred} starts to accumulate when a large fraction of the enzyme has already converted to $H_{red}{}'$ and H^*_{red} is in line with the proposed two-electron reduced nature of this species. Note that the redox state populations plotted in Fig. 2 are normalized, and that the H^*_{red} and H^*_{sred} populations remain minor species when compared to the H_{ox} to $H_{red}{}'$ populations throughout the entire experiment (Fig. S5, ESI†). After photo-reduction, the $H_{red}{}'$ population appears to stay constant for *ca.* 150 seconds. The H^*_{sred} population decays fastest and most probably converts into H^*_{red} whose population is transiently increased before decaying as well (Fig. S4, ESI†). The H_{ox} population remains constant for *ca.* 30 seconds after illumination and recovers subsequently. Similar relatively sluggish conversion from one-electron reduced states to H_{ox} has been observed in group A [FeFe]-hydrogenases before.[63] Thus, the study of *Tam*HydS^{PDT} has allowed us to observe three reduced states $(H_{red}{}', H^*_{red}, H^*_{sred})$, complementing the observation of the H_{red} state previously reported for *Tam*HydS^{ADT}.[9,10]

New redox states for group D [FeFe]-Hydrogenase *Tam*HydS^{ADT}

Performing the analogous photo-reduction experiment on the catalytically active form *Tam*HydS^{ADT} (in the following *Tam*HydS) resulted in more complex spectral changes. In Fig. 3A, difference spectra reflecting changes after 44 seconds (44s–0s, top spectrum) and 220 seconds (220s–0s, middle spectrum) of continuous illumination relative to the starting "pre-illumination" ("0") spectrum are displayed (absolute and full series of difference spectra in Fig. S6, ESI†). As expected, we observe a decrease of bands associated with the oxidized states, H_{ox} and $H_{ox}H$ (grey and dark grey bands). The difference spectra also suggest the de-population of an additional minor species with small negative bands detected at 1960, 1939 and 1782 cm^{-1} (orange bands). These bands are reminiscent of $H_{red}{}'$ when compared to *Tam*HydS^{PDT} (Fig. 2) and group A enzymes,[12,15] implying that this reduced species is present in low amounts at pH 8.

In contrast to the reduction of *Tam*HydS by H_2 gas and electrochemistry as reported earlier,[9,10] we detect two distinct terminal distal CO bands at 1895 and 1875 cm^{-1}. To fit these bands, additional bands at 1887 and 1865 cm^{-1} were necessary, overall indicative of four separate diiron site reduced states. The assignment to four distinct H-cluster states is further strengthened by their independent (de-)population kinetics during the photo-reduction experiment (Fig. 3B). The highest wavenumber band at 1895 cm^{-1} is attributable to the previously observed protonated and reduced diiron site state, H_{red}, with an additional CO band detected at 1922 cm^{-1} and CN^- bands at 2030 and 2062 cm^{-1}. The band at 1887 cm^{-1}, which increases together with a band at 1912 cm^{-1}, is attributed to the two electron reduced state H_{sred}, based on its position relative to that of H_{red} at 1895 cm^{-1} and comparison to the infrared signatures of group A [FeFe]-hydrogenases.[19,25] The possibility that the signals at 1887 and 1895 cm^{-1} instead reflect two H_{red} state populations with different redox states of neighbouring F-clusters is highly unlikely to rationalize the here observed shift of *ca.* 10 cm^{-1}.[64,65] The band at 1875 cm^{-1}, which follows the same kinetics as the bands at 2052, 2012 and 1903 cm^{-1}, can be assigned to H^*_{red}, based on the H^*_{red} state signature observed in *Tam*HydS^{PDT}. Finally, based on the assignment of H^*_{red}, we can assign the small band detected at 1865 cm^{-1} to H^*_{sred}. We note that this implies a blue-shift of the band by about 8 cm^{-1}, when the dithiolate ligand featured an amine bridgehead group relative to the methylene analogue. This would be in good agreement with what has been reported for the group C [FeFe]-hydrogenase *Tm*HydS, for which the band pattern of H^*_{red} in *Tm*HydS^{ADT} shifted to higher wavenumbers by *ca.* 10 cm^{-1} when compared to *Tm*HydS^{PDT}.[3] Chongdar *et al.* attributed this shift to a change in electron density at the diiron core induced by the nature of the bridging dithiolate ligand.

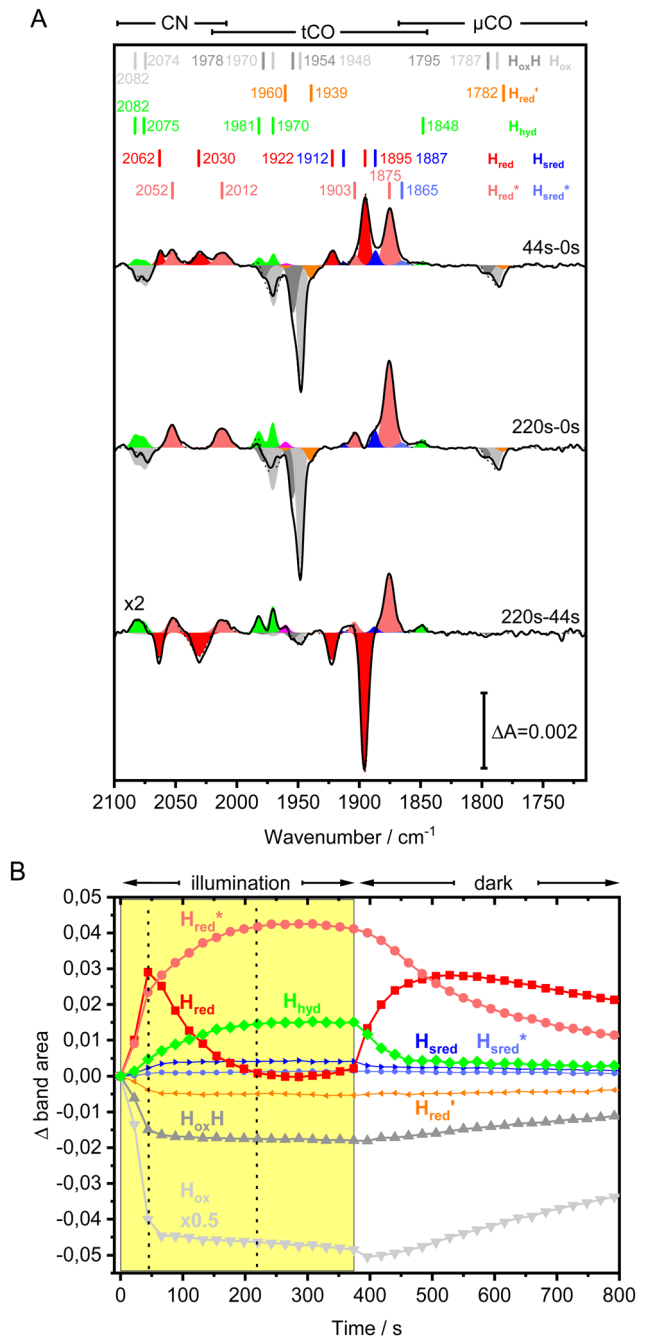

Fig. 3 (A) Light minus dark ATR-FTIR difference spectra of the *Tam*HydS/Eosin Y/TEOA mixture after 44 seconds (top spectrum) and 220 seconds of illumination (middle spectrum). The bottom difference spectrum is calculated between 44 and 220 seconds of illumination (timepoints indicated by vertical dashed lines) where only small changes in oxidized redox states population occur (compare dashed lines in Fig. 3B) enabling the detection of the hydride state bands. The peaks of terminal cyanide (CN), terminal (tCO) and bridging carbon monoxide (μCO) ligands for each different redox state are colour coded, and the band patterns indicated by coloured bars. The difference spectrum is indicated in black and the fit by a dashed line. Upon photo-reduction the oxidized states (H_{ox}, $H_{ox}H$) and H_{red}' depopulate in favour of the one-electron and two electron reduced states (H_{red}, H_{sred}, H^*_{red}, H^*_{sred} and H_{hyd}). Compare to Fig. 3B for the kinetics of (de)-population during and after photo-reduction. An unassigned band is indicated in magenta. (B) Redox state population kinetics during and after photo-reduction of *Tam*HydS. The summed band area of each individual redox state is plotted for visual comparison of the (de)-population kinetics. Within the first 40–60 seconds we observe a depopulation of the oxidized states (H_{ox}, $H_{ox}H$) as well as the one-electron reduced state H_{red}'. The population of H_{red} reaches its maximum after 44 seconds and depopulates subsequently in the expense of H^*_{red} and the two electron reduced states (H_{sred}, H^*_{sred}, H_{hyd}). H_{hyd} seems to accumulate the slowest reaching its maximum around 200 seconds. After photo-reduction, the two-electron reduced protonated redox states H_{hyd} and H_{sred} depopulate at the same time scale as we observe an increase of H_{red}. H^*_{red} (and H^*_{sred}) decay on a slower timescale. The population of H_{ox}, $H_{ox}H$ and H_{red}' remains nearly constant for 80 seconds after photo-reduction. The yellow box indicates the illumination period. Each point is extracted from a difference spectrum (x–0 seconds) (Fig. S6, ESI†) and difference spectra for 44–0, 220–0 and 220–44 seconds are shown in Fig. 3A.

To test this latter hypothesis, regarding the influence of the bridgehead group on the FTIR signatures of the H-cluster, we studied a series of diiron site mimics (Fe(I)Fe(I)) featuring ADT and PDT ligands with different combinations of carbonyl, phosphine and CN^- ligands (Fig. S7, ESI†). The effect of the bridgehead group of the dithiolate ligand was found to vary depending on the rest of the ligand sphere of the model complexes. It was most distinct in the dicyanide complexes, where the mimic featuring the PDT ligand displayed a shift of certain CO bands by 8 cm^{-1} relative to the ADT ligated analogue. When comparing the infrared signatures of *Tam*-$HydS^{PDT}$ and *Tam*$HydS^{ADT}$, a clear effect by H-cluster redox state was found (overview of infrared signatures in Table 1 and Fig. S9, ESI†). The two *Tam*HydS versions seem to be nearly identical for H_{ox} with 0–2 cm^{-1} shifts of the cofactor ligand bands. Conversely, for H_{red}', we observe a 9 cm^{-1} shift on the proximal CO (pCO) band while the distal CO (dCO) band is found at an identical position. While for the H^*_{red} and H^*_{sred} states, the dCO band is shifted by 7–10 cm^{-1} to higher energies in *Tam*$HydS^{ADT}$ relative to *Tam*$HydS^{PDT}$. In combination, these observations support the idea that the nature of the bridgehead can influence the FTIR signature of H-cluster states. However, evidently, the effect is difficult to predict as the effect varies both with oxidation state and the remaining ligand sphere.

As the concentration of H_{ox} states remains practically constant after 44 seconds (Fig. 3B) the difference spectrum calculated between 220 and 44 seconds of illumination (220s–44s, Fig. 3A bottom) has no significant negative contributions from the oxidized state bands between 1980–1948 cm^{-1}. This allows assigning the additional positive bands at 2082, 2075, 1981, 1970 and 1848 cm^{-1} to the CN^- and CO ligands of a redox state with a super-oxidized diiron site when compared to H_{ox}. The inhibited states, H_{inact} and H_{trans}, feature a super-oxidized diiron site. However, reduction reactivates these inhibited states, thus they are highly unlikely to accumulate under photo-reduction.[19,66] Instead we attribute the band pattern to the hydride state, H_{hyd} (positive green bands, Fig. 3 bottom spectrum), which exhibits similar band patterns in group A [FeFe]-hydrogenases.[24,55] However, due to the low population of the putative H_{hyd} species when performing the experiment in D_2O we refrain from a definite assignment.[24,28] Attempts at enriching this proposed essential catalytic intermediate in

*Tam*HydS *via* our group A [FeFe]-hydrogenase specific protocols (low pH value, optional high reductant concentration, and exposure to H_2 gas[24,26]) led to the population of H_{red} only, even though a significant fraction of $H_{ox}H$ was present.[9]

To conclude, we observe similar redox states in group A and D [FeFe]-hydrogenases. The H-cluster in *Tam*HydS can clearly adopt the oxidized state (H_{ox}), the one-electron reduced states H_{red}' and H_{red} with the reducing equivalent on the $[4Fe–4S]_H$ or the diiron site respectively, the super reduced state (H_{sred}) with one reducing equivalent on the $[4Fe–4S]_H$, and the diiron site each, and appears to form also the di-ferrous terminal hydride state (H_{hyd}).

To further investigate the interconversion of these redox states during and after photo-reduction, we again analysed the redox state population changes as a function of time (Fig. 3B). The quantification was done through summation of the areas of the bands associated with each state. The oxidized states H_{ox} and $H_{ox}H$ as well as for the one-electron reduced state, H_{red}' depopulate mainly during the first 44 seconds, and reach a steady concentration after 66 seconds. The protonated one-electron reduced state H_{red} reaches its maximum population after 44 seconds, after which time the population of this species clearly decreases again. The alternative one-electron reduced state H^*_{red} instead increases on a slower timescale (*ca.* 50% populated at 44 s) and reaches a steady-state population after about 220 seconds. As can be seen in Fig. 3A, H_{red} and H^*_{red} are the main reduced states formed during photo-reduction. The two-electron reduced state H_{sred} rise to a plateau population within 120 seconds, while the H_{hyd} population takes approximately double the time (220 seconds, compare as well bottom spectrum Fig. 3A). Notably, the rise of H_{hyd} coincides with the decay of H_{red}. The time-dependency of the H^*_{sred} population is difficult to track with certainty due to the low signal intensity but seem to continuously increase slowly during illumination. Overall, these trends are in good agreement with an increasingly negative solution potential upon extended illumination. After illumination, we observe the converse transitions between H-cluster state populations. The protonated two-electron reduced states, H_{sred} and H_{hyd}, depopulate rapidly (negligible residual signal at $t \approx 420$ s and 460 s, respectively; where illumination is stopped at $t = 374$ s). On a much longer timescale compared to the decay of H_{sred} and H_{hyd} the populations of H^*_{red} (50% de-populated at 500 s) and H^*_{sred} decrease. The population of H_{red} varies in a more complex fashion. Again, coinciding with the opposite kinetics of H_{hyd}, H_{red} increases shortly after illumination is arrested (maximum population at *ca.* 500 s) before it slowly starts to decrease. Similar to *Tam*HydS^{PDT} the population of the oxidized states, H_{ox} and $H_{ox}H$, remain nearly constant for *ca.* 80 seconds and repopulate slowly afterwards. The rapid appearance of H_{red} but more sluggish reformation of the $H_{ox}/H_{ox}H$ after illumination agrees with H_{red} as a quasi-stable resting state as previously noted in H_2 flushing experiments.[9]

Considering the more recently identified H^*_{red} and H^*_{sred} states, and assuming that the structural assignment of H^*_{red} proposed by Chongdar *et al.* is correct,[3] there are at least two possible scenarios that can explain the kinetics observed in this study. H^*_{red}, and the associated H^*_{sred}, state could reflect inhibited states, potentially related to the reductive inhibition phenomena previously noted by Léger and co-workers,[67] or represent catalytically relevant states closely related to the H_{red}' state.

If H^*_{red} would represent an inhibited, off-pathway, species, H_{red} and H_{hyd} would be the main reduced catalytic species interconverting during and after photo reduction. Indeed, the decay of H_{red} during prolonged illumination (photo-reduction) coincides with the population of H_{hyd}. Similar but opposite behaviour is observed directly after photo-reduction; H_{red} gets populated while H_{hyd} de-populates on the same timescale. The kinetics of H^*_{red} do not seem to be following the kinetics of either of these states besides getting populated alongside H_{red} at the beginning of the photo-reduction experiment. During the post-illumination phase, H^*_{red} decays slowly, potentially interconverting into H_{red} after the H_{hyd} state already decayed (around 500 seconds). The accumulation of a large population of an inhibited state under reducing conditions could also partially rationalize the low catalytic activities observed for group C and D [FeFe]-hydrogenases.[3,9] Still, we note that this model would require that the inhibition is reversible on the time-scale of the experiment, as otherwise the H^*_{red} state population would be expected to continuously increase during the photo-reduction. Arguing against this scenario is the fact that no reductive inhibition has been reported from earlier electrochemical studies of *Tam*HydS.[9,49,50] The alternative rationale would be that H^*_{red} *vs.* H_{red} populations are governed by the relative rates of electron transfer and protonation. Here, pure electron transfer would yield H^*_{red}, while coupled (but not necessarily concerted) electron transfer and protonation yields H_{red}. During extended illumination we can expect electron transfer rates to increase as the population of photo-reduced EY increases, while proton transfer rates remain unchanged. This would potentially result in an increase in population of the reduced unprotonated state H^*_{red} relative to H_{red}. As illumination is arrested, the solution potential decreases and the protonation step can now compete, resulting in a decrease of H^*_{red} relative to H_{red}, as observed in our experiments on a longer timescale after illumination is stopped (starting around 500 seconds). This would instead make H^*_{red} a catalytically relevant intermediate analogous but not identical to H_{red}', with still unidentified structural aspects of *Tm*HydS and *Tam*HydS favoring reduction of the di-iron site instead of the [4Fe4S] cluster during the initial electron injection into the H-cluster. The currently available data does not allow us to strictly distinguish these two hypotheses.

We note that when analysing the kinetics of the photo-reduction experiment in isolation, the population of the redox state assigned *via* spectroscopic analysis to H^*_{red} would be intuitively rather assigned to a two electron reduced species *e.g.* H_{sred}. However, such an assignment would imply a down shift of 20 cm^{-1} of the main band of H_{red} (1895 cm^{-1}) to the putative H_{sred} main band (1875 cm^{-1}), contradicting all previous studies involving these two redox states reporting a shift of $\approx$10 cm^{-1}.[12,19,23,25,35,37]

Altering the pH in these photo-reduction assays can significantly affect both the H-cluster kinetics as well as the photochemistry, and should thus be interpreted carefully. Still, to further probe the nature of the species giving rise to the H^*_{red} signature, we performed additional photo-reduction experiments at lower pH (Fig. S6, ESI†). Albeit this data should only be considered qualitative, reduction at lower pH did suppress the 1875 cm^{-1} signal, while the relative amplitude of the H_{red} signature increased, in good agreement with the expected behaviour of the H^*_{red} species.

A bridging CO band in H_{red} observed at room temperature in *Tam*HydS^{ADT}

The FTIR signature of the H_{red} species generated under photo-reduction was consistently shifted to slightly lower energies, relative to our earlier reported data for the H_2 induced H_{red} state.[9] To verify that this was not due to variations in enzyme preparations, we exposed films of *Tam*HydS to a 10% H_2 atmosphere. As expected, this treatment generated difference spectra displaying a nearly exclusive $H_{ox}/H_{ox}H$ to H_{red} (2063, 2032, 1922 and 1896 cm^{-1}) transition, with only residual traces of other redox states being formed (Fig. 4). This verified that the FTIR signature of H_{red} obtained in the photo-reduction experiment was indeed shifted relative to the H_{red} species enriched under H_2, with the latter displaying shifts of the CO and CN^- ligand bands of 1–2 cm^{-1} to higher wavenumbers. Such small but distinct shifts have previously been observed for group A [FeFe]-hydrogenase and have been attributed to differences in the redox states of surrounding F-clusters.[64,65]

To verify this hypothesis, we performed EPR spectroscopy on photo-reduced *Tam*HydS samples. Our earlier EPR studies of *Tam*HydS have shown that H_2 gas exposure only results in partial reduction of the F-clusters. More specifically, H_2 treatment gives rise to one broad rhombic feature, attributable to the reduction of a single [4Fe4S] cluster.[9,47] The photo-reductant employed here resulted in a larger degree of [4Fe4S] cluster reduction, as evident from the appearance of at least two distinct rhombic signals in samples illuminated in the presence of Eosin Y and TEOA (Fig. S8, ESI†).

We note that attempts at fitting the H_{red} state observed during or after photo-reduction (Fig. 3) with two peaks at 1895 and 1896 cm^{-1} excludes the population of the H_2 induced H_{red} state with potentially oxidized F-clusters (Fig. S6, ESI†). More importantly, these H_2 induced H_{red} spectra also display an additional broad but distinct band at 1803 cm^{-1}, which correlates in intensity with the other features of the H_{red} signature. The frequency of this band strongly supports the notion that it reflects a μCO ligand.

A similar μCO band was observed in photo-reduction experiments with *Tam*HydS, showing a nearly exclusive transition from H_{ox} to H_{red}.[68] In these experiments, the μCO band of H_{red} was downshifted by about 1 cm^{-1} compared to the H_2-induced H_{red} state seen here, further supporting our hypothesis of further reduced F-clusters. However, we did not include this band in the analysis in Fig. 3, as it did not improve the fit.

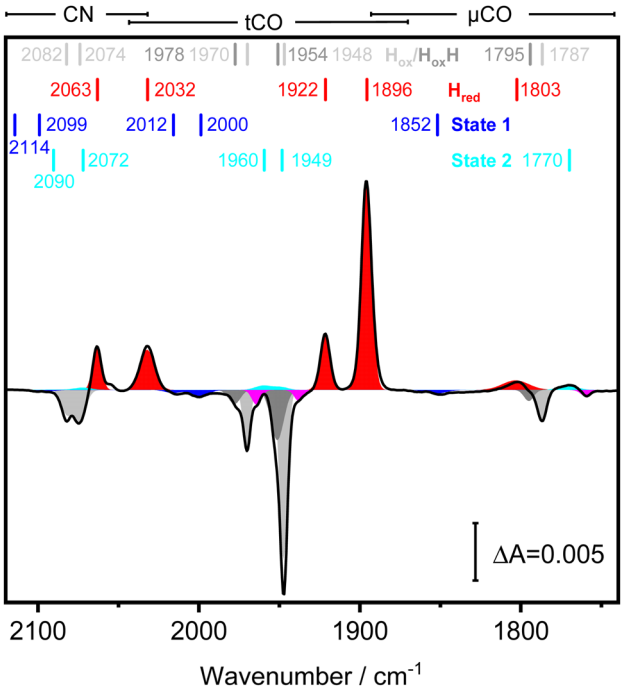

Fig. 4 H_2 induced H_{red} in *Tam*HydS exhibits a potential bridging CO ligand band at ambient conditions. A *Tam*HydS film equilibrated under 2% H_2 (pH 8) was exposed for 44 seconds to 10% H_2 resulting in an increased population of H_{red}. The difference spectrum shows a nearly exclusive $H_{ox}/H_{ox}H$ to H_{red} transition when compared to the rather crowded difference spectra obtained *via* photo-reduction (compare Fig. 3). A band in the bridging CO ligand region at 1803 cm^{-1} co-populates with the bands at 2063, 2032, 1922 and 1896 cm^{-1} and is thus assigned to H_{red}. When compared to the IR signature obtained *via* photo-reduction the bands of H_{red} *via* H_2 exposure are slightly shifted to higher wavenumbers indicative of oxidized F-clusters.[64,65] The spectrum contains trances of State 1 and State 2, described earlier.[47] Magenta peaks indicate residual unassigned species.

Surprisingly, the μCO band of the reduced diiron site (1803 cm^{-1}) is found at higher wavenumbers when compared to the μCO band position of the oxidized state, H_{ox} (1787 cm^{-1}). This high wavenumber position seems counter intuitive for a μCO vibration at a more reduced diiron site, as that should instead induce a significant shift to lower wavenumbers due to increased π back-bonding. As a comparison, the μCO band of the formally super-oxidized state, H_{hyd} (Fe(II)Fe(II)), shifts by *ca.* 60 cm^{-1} to higher wavenumbers when compared to the oxidized state H_{ox} (Fe(II)Fe(I)).[24,55] A comparable up-shift relative to H_{ox} is observed for the inhibited state, H_{inact}, as well.[69] Furthermore, in group C [FeFe]-hydrogenase, *Tm*HydS, the μCO band for the putatively unprotonated reduced state, H^*_{red}, has been reported red shifted by 40 cm^{-1}, relative to H_{ox}, to 1763 cm^{-1}.[3] The fact that H_{red} and H^*_{red} most likely vary in protonation state of the ADT-amine would only partially rationalize the higher energy of the μCO for H_{red} in *Tam*HydS as compared to H^*_{red} in *Tm*HydS,[70,71] as model complexes have consistently shown that protonation of the ADT amine cause a 16–20 cm^{-1} upshift of the CO bands. However, similar high μCO band positions for H_{red} have been observed at cryogenic

temperatures for group A [FeFe]-hydrogenases,[37–39] and correlation of this experimental data with Density Functional Theory calculations favour its attribution to a Fe(I)Fe(I) species with strict rotated μCO geometry and a protonated ADT ligand.[38,72] Summing up, the fact that a band is now observed at this position provides compelling support for the notion that H_{red} can harbour a μCO ligand at room temperature. We further note that the absence of any μCO band in our spectra for H^*_{red} and H^*_{sred} in both the ADT and PDT version of *Tam*HydS differs somewhat from what has been reported for the group C representative *Tm*HydS.[3] In the latter case, the fully functional ADT version of the enzyme did show a distinct μCO band, while no corresponding band was observed for the PDT variant. Evidently, the relative amplitude of the μCO band is strongly dependent on a range of factors including temperature and nature of the bridgehead group.

Conclusions

Besides H_{ox}/H_{ox}H and H_{red}, this study confirms that the H-cluster in *Tam*HydS forms additional redox states analogous to the ones observed for group A [FeFe]-hydrogenases (Table 1 and Fig. S9, ESI†).[5,72] This lends spectroscopy support to the notion that group A and group D [FeFe]-hydrogenases follow the same catalytic cycle, as previously proposed from kinetic fitting of electrochemical data.[49] The idea of a shared catalytic mechanism is further supported by the observed sequential population of key redox states. In this scenario, the slow catalytic kinetics of *Tam*HydS are attributable to an increased stability of H_{red} in the putatively sensory enzymes group C and D hydrogenases, relative to the group A. In the current study, this enhanced stability of H_{red} is reflected in its fast formation upon illumination and relatively slow conversion back to H_{ox} once illumination is stopped (Fig. 3). The stability of the one-electron reduced intermediate over a wide potential range is further in agreement with the spectro-electrochemistry data reported for the group C [FeFe]-hydrogenase *Tm*HydS.[3,48]

However, different mechanisms operating in different groups of [FeFe]-hydrogenases cannot be fully excluded at this stage. The fact that H^*_{red} and H^*_{sred} are found to accumulate in both group C and D [FeFe]-hydrogenases, while no corresponding states have been observed for group A enzymes, underscores that the protein environment induces distinct differences in the properties of the H-cluster between groups. As noted above, one possible explanation for the accumulation of H^*_{red} and H^*_{sred} in these slow [FeFe]-hydrogenases could be that these are inhibited states, which would explain why mainly H_{red}/H_{hyd} populations interconvert during and after photo-reduction. On the other hand, the diiron site is clearly much more easily reduced in these two putatively sensory hydrogenases, as it accumulates without concomitant protonation and the slow interconversion of H_{red}/H^*_{red} after photo-reduction would favour H^*_{red} to be a potential catalytic relevant intermediate. When comparing group D and A enzymes the differences in H-cluster reactivity are further evidenced by the fact that still incompletely characterized spectroscopic features have been observed in *Tam*HydS under H_2 pressure.[9,47] Beside reporting numerous H-cluster states previously unidentified in group D, our study sheds new light on the common H_{red} intermediate. Besides group C, this species appears to be shared across all [FeFe]-hydrogenases studied to date, but its structural details remain contested. The data reported herein does not allow for definite distinction between models 1 or 2, as direct experimental proof of either a μH ligand or a protonation of the ADT ligand (Fig. 1B) remains elusive. Still, when the diiron site reduced state, H_{red}, is induced *via* exposure to H_2 gas in *Tam*HydS, we now observe a band in the μCO band region that appears to be associated with H_{red}, indicating the existence of a bridging CO ligand in the H_{red} state at room temperature in line with the recent report of a μCO band for photo-reduced *Tam*HydS.[68] We note that in earlier reports of group A [FeFe]-hydrogenases traces of a μCO bands potentially attributable to the H_{red} state could be visible at room temperatures as well, but to the best of our knowledge this is the first reported instance where the band is so clearly discernible. We show that H_{red} can adopt different F-cluster redox configurations, and the retained rotated diiron site geometry implied from the μCO band at ambient temperature would render H_{red} a potential catalytic intermediate.

In closing, we stress that many details surrounding the catalytic mechanism(s) of [FeFe]-hydrogenase remain to be resolved. However, the fact that H_{ox}, $H_{red}{}'$, H_{red}, H_{sred} and H_{hyd}, have now all been observed in both group A and D [FeFe]-hydrogenase, arguably suggests a shared catalytic cycle. In addition, the here observed μCO ligand in H_{red}, favours a catalytic cycle involving diiron site reduced intermediates. Overall, these findings highlight how studies of [FeFe]-hydrogenases from alternative groups can provide new insight into the catalytic cycle, underscoring the need for continuous exploration of this diverse and fascinating enzyme family.

Author contributions

M. S. designed experiments, performed the FTIR spectroscopy, analysed data and wrote the first draft of the manuscript. C. S. and P. H. performed EPR spectroscopy and analysed data. A. Z. performed the synthesis work. C. S., P. R. C. and H. L. isolated the proteins. G. B. contributed to the data analysis and manuscript preparation. All authors were involved in the analysis and revision of the manuscript and have given approval to the final version of the manuscript.

Data availability

The methods and data supporting the findings of this study are available in the ESI.†

Conflicts of interest

There are no conflicts to declare.

Acknowledgements

The authors would like to thank Leopold Fichet for his contributions to the FTIR spectroscopy experiments. The work presented in this article is supported by the Novo Nordisk Foundation (NNF23OC0085682 to MS) and by the Swedish Research Council (2023-04593 to MS, 2021-04471 to GB). The Swedish Energy Agency (STEM, grant no 48574-1 to GB), the Olle Engkvist stiftelse (grant no 220-0226 to GB and MS) and the European Union Horizon Europe - the Framework Programme for Research and Innovation (2021–2027) under the grant agreement number 101070948 (project PhotoSynH2 to GB) are gratefully acknowledged for funding.

Notes and references

1 C. Greening, P. R. Cabotaje, L. E. Valentin Alvarado, P. M. Leung, H. Land, T. Rodrigues-Oliveira, R. I. Ponce-Toledo, M. Senger, M. A. Klamke, M. Milton, R. Lappan, S. Mullen, J. West-Roberts, J. Mao, J. Song, M. Schoelmerich, C. W. Stairs, C. Schleper, R. Grinter, A. Spang, J. F. Banfield and G. Berggren, Minimal and hybrid hydrogenases are active from archaea, *Cell*, 2024, **187**(3357–3372), e3319.

2 H. Land, M. Senger, G. Berggren and S. T. Stripp, Current State of [FeFe]-Hydrogenase Research: Biodiversity and Spectroscopic Investigations, *ACS Catal.*, 2020, **10**, 7069–7086.

3 N. Chongdar, J. A. Birrell, K. Pawlak, C. Sommer, E. J. Reijerse, O. Rudiger, W. Lubitz and H. Ogata, Unique Spectroscopic Properties of the H-Cluster in a Putative Sensory [FeFe] Hydrogenase, *J. Am. Chem. Soc.*, 2018, **140**, 1057–1068.

4 S. T. Stripp, B. R. Duffus, V. Fourmond, C. Leger, S. Leimkuhler, S. Hirota, Y. Hu, A. Jasniewski, H. Ogata and M. W. Ribbe, Second and Outer Coordination Sphere Effects in Nitrogenase, Hydrogenase, Formate Dehydrogenase, and CO Dehydrogenase, *Chem. Rev.*, 2022, **122**, 11900–11973.

5 J. T. Kleinhaus, F. Wittkamp, S. Yadav, D. Siegmund and U. P. Apfel, [FeFe]-Hydrogenases: maturation and reactivity of enzymatic systems and overview of biomimetic models, *Chem. Soc. Rev.*, 2021, **50**, 1668–1784.

6 T. R. Simmons, G. Berggren, M. Bacchi, M. Fontecave and V. Artero, Mimicking hydrogenases: From biomimetics to artificial enzymes, *Coordin. Chem. Rev.*, 2014, **270**, 127–150.

7 N. Kornienko, J. Z. Zhang, K. K. Sakimoto, P. Yang and E. Reisner, Interfacing nature's catalytic machinery with synthetic materials for semi-artificial photosynthesis, *Nat. Nanotechnol.*, 2018, **13**, 890–899.

8 W. Lubitz, H. Ogata, O. Rudiger and E. Reijerse, Hydrogenases, *Chem. Rev.*, 2014, **114**, 4081–4148.

9 H. Land, A. Sekretareva, P. Huang, H. J. Redman, B. Nemeth, N. Polidori, L. S. Meszaros, M. Senger, S. T. Stripp and G. Berggren, Characterization of a putative sensory [FeFe]-hydrogenase provides new insight into the role of the active site architecture, *Chem. Sci.*, 2020, **11**, 12789–12801.

10 H. Land, P. Ceccaldi, L. S. Meszaros, M. Lorenzi, H. J. Redman, M. Senger, S. T. Stripp and G. Berggren, Discovery of novel [FeFe]-hydrogenases for biocatalytic H(2)-production, *Chem. Sci.*, 2019, **10**, 9941–9948.

11 J. Esselborn, N. Muraki, K. Klein, V. Engelbrecht, N. Metzler-Nolte, U. P. Apfel, E. Hofmann, G. Kurisu and T. Happe, A structural view of synthetic cofactor integration into [FeFe]-hydrogenases, *Chem. Sci.*, 2016, **7**, 959–968.

12 C. Sommer, A. Adamska-Venkatesh, K. Pawlak, J. A. Birrell, O. Rudiger, E. J. Reijerse and W. Lubitz, Proton Coupled Electronic Rearrangement within the H-Cluster as an Essential Step in the Catalytic Cycle of [FeFe] Hydrogenases, *J. Am. Chem. Soc.*, 2017, **139**, 1440–1443.

13 F. Sievers, A. Wilm, D. Dineen, T. J. Gibson, K. Karplus, W. Li, R. Lopez, H. McWilliam, M. Remmert, J. Soding, J. D. Thompson and D. G. Higgins, Fast, scalable generation of high-quality protein multiple sequence alignments using Clustal Omega, *Mol. Syst. Biol.*, 2011, **7**, 539.

14 C. Greening, A. Biswas, C. R. Carere, C. J. Jackson, M. C. Taylor, M. B. Stott, G. M. Cook and S. E. Morales, Genomic and metagenomic surveys of hydrogenase distribution indicate H2 is a widely utilised energy source for microbial growth and survival, *ISME J.*, 2016, **10**, 761–777.

15 K. Laun, I. Baranova, J. Duan, L. Kertess, F. Wittkamp, U. P. Apfel, T. Happe, M. Senger and S. T. Stripp, Site-selective protonation of the one-electron reduced cofactor in [FeFe]-hydrogenase, *Dalton Trans.*, 2021, **50**, 3641–3650.

16 J. A. Birrell, P. Rodríguez-Maciá, E. J. Reijerse, M. A. Martini and W. Lubitz, The catalytic cycle of [FeFe] hydrogenase: A tale of two sites, *Coordin. Chem. Rev.*, 2021, **449**, 214191.

17 J. H. Artz, O. A. Zadvornyy, D. W. Mulder, S. M. Keable, A. E. Cohen, M. W. Ratzloff, S. G. Williams, B. Ginovska, N. Kumar, J. Song, S. E. McPhillips, C. M. Davidson, A. Y. Lyubimov, N. Pence, G. J. Schut, A. K. Jones, S. M. Soltis, M. W. W. Adams, S. Raugei, P. W. King and J. W. Peters, Tuning Catalytic Bias of Hydrogen Gas Producing Hydrogenases, *J. Am. Chem. Soc.*, 2020, **142**, 1227–1235.

18 M. Senger, S. Mebs, J. Duan, O. Shulenina, K. Laun, L. Kertess, F. Wittkamp, U. P. Apfel, T. Happe, M. Winkler, M. Haumann and S. T. Stripp, Protonation/reduction dynamics at the [4Fe-4S] cluster of the hydrogen-forming cofactor in [FeFe]-hydrogenases, *Phys. Chem. Chem. Phys.*, 2018, **20**, 3128–3140.

19 W. Roseboom, A. L. De Lacey, V. M. Fernandez, E. C. Hatchikian and S. P. Albracht, The active site of the [FeFe]-hydrogenase from Desulfovibrio desulfuricans. II. Redox properties, light sensitivity and CO-ligand exchange as observed by infrared spectroscopy, *J. Biol. Inorg. Chem.*, 2006, **11**, 102–118.

20 J. W. Peters, W. N. Lanzilotta, B. J. Lemon and L. C. Seefeldt, X-ray crystal structure of the Fe-only hydrogenase (CpI) from Clostridium pasteurianum to 1.8 angstrom resolution, *Science*, 1998, **282**, 1853–1858.

21 Y. Nicolet, C. Piras, P. Legrand, C. E. Hatchikian and J. C. Fontecilla-Camps, Desulfovibrio desulfuricans iron hydrogenase: the structure shows unusual coordination to an active site Fe binuclear center, *Structure*, 1999, **7**, 13–23.

22 M. L. Singleton, N. Bhuvanesh, J. H. Reibenspies and M. Y. Darensbourg, Synthetic support of de novo design: sterically bulky [FeFe]-hydrogenase models, *Angew. Chem., Int. Ed.*, 2008, **47**, 9492–9495.
23 S. Katz, J. Noth, M. Horch, H. S. Shafaat, T. Happe, P. Hildebrandt and I. Zebger, Vibrational spectroscopy reveals the initial steps of biological hydrogen evolution, *Chem. Sci.*, 2016, **7**, 6746–6752.
24 M. Winkler, M. Senger, J. Duan, J. Esselborn, F. Wittkamp, E. Hofmann, U. P. Apfel, S. T. Stripp and T. Happe, Accumulating the hydride state in the catalytic cycle of [FeFe]-hydrogenases, *Nat. Commun.*, 2017, **8**, 16115.
25 A. Silakov, C. Kamp, E. Reijerse, T. Happe and W. Lubitz, Spectroelectrochemical characterization of the active site of the [FeFe] hydrogenase HydA1 from Chlamydomonas reinhardtii, *Biochemistry*, 2009, **48**, 7780–7786.
26 M. Senger, T. Kernmayr, M. Lorenzi, H. J. Redman and G. Berggren, Hydride state accumulation in native [FeFe]-hydrogenase with the physiological reductant H(2) supports its catalytic relevance, *Chem. Commun.*, 2022, **58**, 7184–7187.
27 L. S. Meszaros, P. Ceccaldi, M. Lorenzi, H. J. Redman, E. Pfitzner, J. Heberle, M. Senger, S. T. Stripp and G. Berggren, Spectroscopic investigations under whole-cell conditions provide new insight into the metal hydride chemistry of [FeFe]-hydrogenase, *Chem. Sci.*, 2020, **11**, 4608–4617.
28 D. W. Mulder, M. W. Ratzloff, M. Bruschi, C. Greco, E. Koonce, J. W. Peters and P. W. King, Investigations on the role of proton-coupled electron transfer in hydrogen activation by [FeFe]-hydrogenase, *J. Am. Chem. Soc.*, 2014, **136**, 15394–15402.
29 M. Haumann and S. T. Stripp, The Molecular Proceedings of Biological Hydrogen Turnover, *Acc. Chem. Res.*, 2018, **51**, 1755–1763.
30 F. Wittkamp, M. Senger, S. T. Stripp and U. P. Apfel, [FeFe]-Hydrogenases: recent developments and future perspectives, *Chem. Commun.*, 2018, **54**, 5934–5942.
31 J. W. Sidabras and S. T. Stripp, A personal account on 25 years of scientific literature on [FeFe]-hydrogenase, *J. Biol. Inorg. Chem.*, 2023, **28**, 355–378.
32 M. Bruschi, C. Greco, M. Kaukonen, P. Fantucci, U. Ryde and L. De Gioia, Influence of the [2Fe]H subcluster environment on the properties of key intermediates in the catalytic cycle of [FeFe] hydrogenases: hints for the rational design of synthetic catalysts, *Angew. Chem., Int. Ed.*, 2009, **48**, 3503–3506.
33 G. Filippi, F. Arrigoni, L. Bertini, L. De Gioia and G. Zampella, DFT dissection of the reduction step in H2 catalytic production by [FeFe]-hydrogenase-inspired models: can the bridging hydride become more reactive than the terminal isomer?, *Inorg. Chem.*, 2015, **54**, 9529–9542.
34 S. Mebs, R. Kositzki, J. Duan, L. Kertess, M. Senger, F. Wittkamp, U. P. Apfel, T. Happe, S. T. Stripp, M. Winkler and M. Haumann, Hydrogen and oxygen trapping at the H-cluster of [FeFe]-hydrogenase revealed by site-selective spectroscopy and QM/MM calculations, *Biochim. Biophys. Acta, Bioenerg.*, 2018, **1859**, 28–41.
35 S. Mebs, M. Senger, J. Duan, F. Wittkamp, U. P. Apfel, T. Happe, M. Winkler, S. T. Stripp and M. Haumann, Bridging Hydride at Reduced H-Cluster Species in [FeFe]-Hydrogenases Revealed by Infrared Spectroscopy, Isotope Editing, and Quantum Chemistry, *J. Am. Chem. Soc.*, 2017, **139**, 12157–12160.
36 P. Chernev, C. Lambertz, N. Leidel, K. Sigfridsson, R. Kositzki, T. Happe and M. Haumann, Hydride binding to the active-site H-cluster of [FeFe]-hydrogenase, *J. Biol. Inorg. Chem.*, 2014, **19**, S758.
37 M. W. Ratzloff, J. H. Artz, D. W. Mulder, R. T. Collins, T. E. Furtak and P. W. King, CO-Bridged H-Cluster Intermediates in the Catalytic Mechanism of [FeFe]-Hydrogenase CaI, *J. Am. Chem. Soc.*, 2018, **140**, 7623–7628.
38 J. A. Birrell, V. Pelmenschikov, N. Mishra, H. Wang, Y. Yoda, K. Tamasaku, T. B. Rauchfuss, S. P. Cramer, W. Lubitz and S. DeBeer, Spectroscopic and Computational Evidence that [FeFe] Hydrogenases Operate Exclusively with CO-Bridged Intermediates, *J. Am. Chem. Soc.*, 2020, **142**, 222–232.
39 C. Lorent, S. Katz, J. Duan, C. J. Kulka, G. Caserta, C. Teutloff, S. Yadav, U. P. Apfel, M. Winkler, T. Happe, M. Horch and I. Zebger, Shedding Light on Proton and Electron Dynamics in [FeFe] Hydrogenases, *J. Am. Chem. Soc.*, 2020, **142**, 5493–5497.
40 M. Winkler, J. Esselborn and T. Happe, Molecular basis of [FeFe]-hydrogenase function: an insight into the complex interplay between protein and catalytic cofactor, *Biochim. Biophys. Acta*, 2013, **1827**, 974–985.
41 H. J. Redman, P. Huang, M. Haumann, M. H. Cheah and G. Berggren, Lewis acid protection turns cyanide containing [FeFe]-hydrogenase mimics into proton reduction catalysts, *Dalton Trans.*, 2022, **51**, 4634–4643.
42 P. R. Cabotaje, A. Sekretareva, M. Senger, P. Huang, K. Walter, H. J. Redman, N. Croy, S. T. Stripp, H. Land and G. Berggren, Probing the Influence of the Protein Scaffold on H-Cluster Reactivity via Gain-of-Function Studies horizontal line Improved H(2) Evolution and O(2) Tolerance through Rational Design of [FeFe] Hydrogenase, *J. Am. Chem. Soc.*, 2025, **147**, 4654–4666.
43 O. Lampret, A. Adamska-Venkatesh, H. Konegger, F. Wittkamp, U. P. Apfel, E. J. Reijerse, W. Lubitz, O. Rudiger, T. Happe and M. Winkler, Interplay between CN(-) Ligands and the Secondary Coordination Sphere of the H-Cluster in [FeFe]-Hydrogenases, *J. Am. Chem. Soc.*, 2017, **139**, 18222–18230.
44 J. Duan, M. Senger, J. Esselborn, V. Engelbrecht, F. Wittkamp, U. P. Apfel, E. Hofmann, S. T. Stripp, T. Happe and M. Winkler, Crystallographic and spectroscopic assignment of the proton transfer pathway in [FeFe]-hydrogenases, *Nat. Commun.*, 2018, **9**, 4726.
45 M. Senger, V. Eichmann, K. Laun, J. Duan, F. Wittkamp, G. Knor, U. P. Apfel, T. Happe, M. Winkler, J. Heberle and S. T. Stripp, How [FeFe]-Hydrogenase Facilitates Bidirectional Proton Transfer, *J. Am. Chem. Soc.*, 2019, **141**, 17394–17403.
46 L. S. Mészáros, H. Land, H. J. Redman and G. Berggren, Semi-synthetic hydrogenases—in vitro and in vivo applications, *Curr. Opin. Green Sustainable Chem.*, 2021, **32**, 100521.
47 P. R. Cabotaje, K. Walter, A. Zamader, P. Huang, F. Ho, H. Land, M. Senger and G. Berggren, Probing Substrate Transport Effects on Enzymatic Hydrogen Catalysis: An

Alternative Proton Transfer Pathway in Putatively Sensory [FeFe] Hydrogenase, *ACS Catal.*, 2023, **13**, 10435–10446.

48 N. Chongdar, P. Rodriguez-Macia, E. J. Reijerse, W. Lubitz, H. Ogata and J. A. Birrell, Redox tuning of the H-cluster by second coordination sphere amino acids in the sensory [FeFe] hydrogenase from Thermotoga maritima, *Chem. Sci.*, 2023, **14**, 3682–3692.

49 A. Fasano, C. Baffert, C. Schumann, G. Berggren, J. A. Birrell, V. Fourmond and C. Leger, Kinetic Modeling of the Reversible or Irreversible Electrochemical Responses of FeFe-Hydrogenases, *J. Am. Chem. Soc.*, 2024, **146**, 1455–1466.

50 A. Fasano, H. Land, V. Fourmond, G. Berggren and C. Leger, Reversible or Irreversible Catalysis of H(+)/H(2) Conversion by FeFe Hydrogenases, *J. Am. Chem. Soc.*, 2021, **143**, 20320–20325.

51 F. Vincent, P. Nicolas and L. Christophe, Reversible catalysis, *Nat. Rev. Chem.*, 2021, **5**, 348–360.

52 K. Holá, M. V. Pavliuk, B. Németh, P. Huang, L. Zdrazil, H. Land, G. Berggren and H. N. Tian, Carbon Dots and [FeFe] Hydrogenase Biohybrid Assemblies for Efficient Light-Driven Hydrogen Evolution, *ACS Catal.*, 2020, **10**, 9943–9952.

53 D. Adam, L. Bosche, L. Castaneda-Losada, M. Winkler, U. P. Apfel and T. Happe, Sunlight-Dependent Hydrogen Production by Photosensitizer/Hydrogenase Systems, *ChemSusChem*, 2017, **10**, 894–902.

54 M. V. Pavliuk, M. Lorenzi, D. R. Morado, L. Gedda, S. Wrede, S. H. Mejias, A. Liu, M. Senger, S. Glover, K. Edwards, G. Berggren and H. Tian, Polymer Dots as Photoactive Membrane Vesicles for [FeFe]-Hydrogenase Self-Assembly and Solar-Driven Hydrogen Evolution, *J. Am. Chem. Soc.*, 2022, **144**, 13600–13611.

55 M. W. Ratzloff, M. B. Wilker, D. W. Mulder, C. E. Lubner, H. Hamby, K. A. Brown, G. Dukovic and P. W. King, Activation Thermodynamics and H/D Kinetic Isotope Effect of the H(ox) to H(red)H(+) Transition in [FeFe] Hydrogenase, *J. Am. Chem. Soc.*, 2017, **139**, 12879–12882.

56 Y. Honda, Y. Shinohara and H. Fujii, Visible light-driven, external mediator-free H2 production by a combination of a photosensitizer and a whole-cell biocatalyst: Escherichia coli expressing [FeFe]-hydrogenase and maturase genes, *Catal. Sci. Technol.*, 2020, **10**, 6006–6012.

57 M. Lorenzi, M. T. Gamache, H. J. Redman, H. Land, M. Senger and G. Berggren, Light-Driven [FeFe] Hydrogenase Based H(2) Production in E. coli: A Model Reaction for Exploring E. coli Based Semiartificial Photosynthetic Systems, *ACS Sustainable Chem. Eng.*, 2022, **10**, 10760–10767.

58 M. L. K. Sanchez, C. Sommer, E. Reijerse, J. A. Birrell, W. Lubitz and R. B. Dyer, Investigating the Kinetic Competency of CrHydA1 [FeFe] Hydrogenase Intermediate States via Time-Resolved Infrared Spectroscopy, *J. Am. Chem. Soc.*, 2019, **141**, 16064–16070.

59 A. Adamska-Venkatesh, D. Krawietz, J. Siebel, K. Weber, T. Happe, E. Reijerse and W. Lubitz, New redox states observed in [FeFe] hydrogenases reveal redox coupling within the H-cluster, *J. Am. Chem. Soc.*, 2014, **136**, 11339–11346.

60 M. Senger, K. Laun, F. Wittkamp, J. Duan, M. Haumann, T. Happe, M. Winkler, U. P. Apfel and S. T. Stripp, Proton-Coupled Reduction of the Catalytic [4Fe-4S] Cluster in [FeFe]-Hydrogenases, *Angew. Chem., Int. Ed.*, 2017, **56**, 16503–16506.

61 M. Sensi, C. Baffert, V. Fourmond, L. de Gioia, L. Bertini and C. Léger, Photochemistry and photoinhibition of the H-cluster of FeFe hydrogenases, *Sustainable Energy Fuels*, 2021, **5**, 4248–4260.

62 M. Senger, S. Mebs, J. Duan, F. Wittkamp, U. P. Apfel, J. Heberle, M. Haumann and S. T. Stripp, Stepwise isotope editing of [FeFe]-hydrogenases exposes cofactor dynamics, *Proc. Natl. Acad. Sci. U. S. A.*, 2016, **113**, 8454–8459.

63 J. F. Duan, S. Mebs, K. Laun, F. Wittkamp, J. Heberle, T. Happe, E. Hofmann, U. P. Apfel, M. Winkler, M. Senger, M. Haumann and S. T. Stripp, Geometry of the Catalytic Active Site in [FeFe]-Hydrogenase Is Determined by Hydrogen Bonding and Proton Transfer, *ACS Catal.*, 2019, **9**, 9140–9149.

64 P. Rodríguez-Maciá, N. Breuer, S. DeBeer and J. A. Birrell, Insight into the Redox Behavior of the [4Fe–4S] Subcluster in [FeFe] Hydrogenases, *ACS Catal.*, 2020, **10**, 13084–13095.

65 P. Rodriguez-Macia, K. Pawlak, O. Rudiger, E. J. Reijerse, W. Lubitz and J. A. Birrell, Intercluster Redox Coupling Influences Protonation at the H-cluster in [FeFe] Hydrogenases, *J. Am. Chem. Soc.*, 2017, **139**, 15122–15134.

66 P. Rodriguez-Macia, E. J. Reijerse, M. van Gastel, S. DeBeer, W. Lubitz, O. Rudiger and J. A. Birrell, Sulfide Protects [FeFe] Hydrogenases From O(2), *J. Am. Chem. Soc.*, 2018, **140**, 9346–9350.

67 V. Hajj, C. Baffert, K. Sybirna, I. Meynial-Salles, P. Soucaille, H. Bottin, V. Fourmond and C. Léger, FeFe hydrogenase reductive inactivation and implication for catalysis, *Energy Environ. Sci.*, 2014, **7**, 715–719.

68 I. Voloshyn, C. Schumann, P. R. Cabotaje, A. Zamader, H. Land and M. Senger, Secondary structure changes as the potential H(2) sensing mechanism of group D [FeFe]-hydrogenases, *Chem. Commun.*, 2024, **60**, 10914–10917.

69 P. Rodriguez-Macia, L. M. Galle, R. Bjornsson, C. Lorent, I. Zebger, Y. Yoda, S. P. Cramer, S. DeBeer, I. Span and J. A. Birrell, Caught in the H(inact): Crystal Structure and Spectroscopy Reveal a Sulfur Bound to the Active Site of an O(2) -stable State of [FeFe] Hydrogenase, *Angew. Chem., Int. Ed.*, 2020, **59**, 16786–16794.

70 G. Eilers, L. Schwartz, M. Stein, G. Zampella, L. de Gioia, S. Ott and R. Lomoth, Ligand versus metal protonation of an iron hydrogenase active site mimic, *Chemistry*, 2007, **13**, 7075–7084.

71 J. D. Lawrence, H. Li, T. B. Rauchfuss, M. Benard and M. M. Rohmer, Diiron Azadithiolates as Models for the Iron-Only Hydrogenase Active Site: Synthesis, Structure, and Stereoelectronics This research was supported by the NIH and the Centre Universitaire et Regional de Ressources Informatiques of ULP and CNRS, *Angew. Chem., Int. Ed.*, 2001, **40**, 1768–1771.

72 S. T. Stripp, S. Mebs and M. Haumann, Temperature Dependence of Structural Dynamics at the Catalytic Cofactor of [FeFe]-hydrogenase, *Inorg. Chem.*, 2020, **59**, 16474–16488.